HERMES: A DEFICIT IN THE SURFACE BRIGHTNESS OF THE COSMIC INFRARED BACKGROUND DUE TO GALAXY CLUSTER GRAVITATIONAL LENSING[†]

M. Zemcov[1,2], A. Blain[3], A. Cooray[4,1], M. Béthermin[5,6], J. Bock[1,2], D.L. Clements[7], A. Conley[8], L. Conversi[9], C.D. Dowell[1,2], D. Farrah[10,11], J. Glenn[12,8], M. Griffin[13], M. Halpern[14], E. Jullo[15], J.-P. Kneib[16,15], G. Marsden[14], H.T. Nguyen[2,1], S.J. Oliver[10], J. Richard[17], I.G. Roseboom[10,18], B. Schulz[1,19], Douglas Scott[14], D.L. Shupe[1,19], A.J. Smith[10], I. Valtchanov[9], M. Viero[1], L. Wang[10], J. Wardlow[4]

Submitted to ApJL March 26, 2013.

ABSTRACT

We have observed four massive galaxy clusters with the SPIRE instrument on the *Herschel Space Observatory* and measure a deficit of surface brightness within their central region after removing detected sources. We simulate the effects of instrumental sensitivity and resolution, the source population, and the lensing effect of the clusters to estimate the shape and amplitude of the deficit. The amplitude of the central deficit is a strong function of the surface density and flux distribution of the background sources. We find that for the current best fitting faint end number counts, and excellent lensing models, the most likely amplitude of the central deficit is the full intensity of the cosmic infrared background (CIB). Our measurement leads to a lower limit to the integrated total intensity of the CIB of $I_{250\,\mu m} > 0.69^{+0.03}_{-0.03}(\text{stat.})^{+0.11}_{-0.06}(\text{sys.})\,\text{MJy sr}^{-1}$, with more CIB possible from both low-redshift sources and from sources within the target clusters. It should be possible to observe this effect in existing high angular resolution data at other wavelengths where the CIB is bright, which would allow tests of models of the faint source component of the CIB.

Subject headings: cosmic background radiation

zemcov@caltech.edu

[†] Herschel is an ESA space observatory with science instruments provided by European-led Principal Investigator consortia and with important participation from NASA.
[1] California Institute of Technology, 1200 E. California Blvd., Pasadena, CA 91125
[2] Jet Propulsion Laboratory, 4800 Oak Grove Drive, Pasadena, CA 91109
[3] Physics & Astronomy, University of Leicester, University Road, Leicester, LE1 7RH, UK
[4] Dept. of Physics & Astronomy, University of California, Irvine, CA 92697
[5] Laboratoire AIM-Paris-Saclay, CEA/DSM/Irfu - CNRS - Université Paris Diderot, CE-Saclay, pt courrier 131, F-91191 Gif-sur-Yvette, France
[6] Institut d'Astrophysique Spatiale (IAS), bâtiment 121, Université Paris-Sud 11 and CNRS (UMR 8617), 91405 Orsay, France
[7] Astrophysics Group, Imperial College London, Blackett Laboratory, Prince Consort Road, London SW7 2AZ, UK
[8] Center for Astrophysics and Space Astronomy 389-UCB, University of Colorado, Boulder, CO 80309
[9] Herschel Science Centre, European Space Astronomy Centre, Villanueva de la Cañada, 28691 Madrid, Spain
[10] Astronomy Centre, Dept. of Physics & Astronomy, University of Sussex, Brighton BN1 9QH, UK
[11] Department of Physics, Virginia Tech, Blacksburg, VA 24061
[12] Dept. of Astrophysical and Planetary Sciences, CASA 389-UCB, University of Colorado, Boulder, CO 80309
[13] School of Physics and Astronomy, Cardiff University, Queens Buildings, The Parade, Cardiff CF24 3AA, UK
[14] Department of Physics & Astronomy, University of British Columbia, 6224 Agricultural Road, Vancouver, BC V6T 1Z1, Canada
[15] Aix-Marseille Université, CNRS, LAM (Laboratoire d'Astrophysique de Marseille) UMR7326, 13388, France
[16] Laboratoire d'Astrophysique, Ecole Polytechnique Federale de Lausanne (EPFL), Observatoire de Sauverny, CH-1290 Versoix, Switzerland
[17] Centre de Recherche Astronomique de Lyon, Université Lyon 1, 9 avenueCharles André, F-69230 Saint-Genis Laval, France; CNRS, UMR 5574; Ecole Normale Supérieure de Lyon, Lyon, France
[18] Institute for Astronomy, University of Edinburgh, Royal Observatory, Blackford Hill, Edinburgh EH9 3HJ, UK
[19] Infrared Processing and Analysis Center, MS 100-22, California Institute of Technology, JPL, Pasadena, CA 91125

1. INTRODUCTION

The effect of gravitational lensing is to redistribute the intensity from sources behind the lens into images with different positions and brightnesses, while conserving surface brightness (Schneider et al. 1992). This means that gravitational lensing not only magnifies the background sources, but also changes their apparent density on the sky. The details of whether the number counts of background sources seen through a foreground gravitational lens such as a galaxy cluster are increased or decreased depend on the properties of the lens and the slope of the faint counts (Refregier & Loeb 1997), a process known as magnification bias (Turner 1980).

In this letter, we report detection of a deficit in the surface brightness of the cosmic infrared background (CIB) in the centers of massive galaxy clusters measured using the SPIRE instrument (Griffin et al. 2010) on the *Herschel Space Observatory* (Pilbratt et al. 2010). To interpret these observations and understand the consequences of lensing a background field, the lensing properties of the cluster and the background source population are carefully simulated in a large number of realizations. We concentrate on the intensity profile after removing detected sources to highlight faint fluctuations in the CIB. The resulting effect after such a removal is a localized region of decreased surface brightness at the cluster center. The fluctuations are modulated in our maps due to the resolution of the SPIRE instrument, ~ 20 arcsec. We

use these observations to constrain the intensity of the sub-mm background at $250\,\mu$m.

2. OBSERVATION OF THE DEFICIT

This study uses confusion-limited maps of galaxy clusters from the *Herschel* Multi-tiered Extragalactic Survey (HerMES; HerMES Collaboration et al. 2012). The SPIRE data are reduced using a combination of the HIPE (Ott et al. 2006) and SMAP (Levenson et al. 2010; Viero et al. 2012) packages[1]. The sample of clusters is listed in HerMES Collaboration et al. (2012) and Zemcov et al. (in preparation).

In order to study the strongly lensed regions it is necessary to restrict our attention to those clusters large enough that $\Omega_c > 3\Omega_s$, where Ω_c is the solid angle of the negative magnification region and Ω_s is the solid angle of the SPIRE beam. This cut leaves only the four clusters from the HerMES sample of twelve: Abell 370, Abell 1689, Abell 2219 and RX J1347−1145. The negative magnification region in the image plane maps to the interior of the lens caustic in the source plane, so it is a reasonable tracer of the area which undergoes strong magnification and large deflections by the lensing system. The mapping from total mass to lensing characteristics is complex and the area Ω_c is not strictly proportional to cluster mass; however, this cut does effectively restrict our analysis to the most massive centrally-condensed systems.

To measure the deficit, a catalog is generated for each cluster at each SPIRE wavelength using the SCAT algorithm (Smith et al. 2012) based on $250\,\mu$m source-selection. Our goal is not to identify particular point sources, but rather to make a catalog which aids in removing emission from point sources to reveal the diffuse structure. Thus, employing a low detection threshold is reasonable. We chose a 1σ threshold, where σ is the map root-mean-square variation, dominated in these deep maps by confusion noise. The measurement is not sensitive to the precise value of this number provided it is not so high as to leave residual sources ($> 3\sigma$) nor so low as to needlessly mask a large fraction of the map ($< 0.5\sigma$). This yields a catalog of ~ 500 sources in each cluster field which are then subtracted from the cluster image using a Gaussian model of the beam. An example of the resulting image for one cluster is shown in Fig. 1, which shows a statistical deficit in surface brightness near the center of the cluster. A simple way to visualize this deficit is to plot annular averages of the source-subtracted maps, as shown in Fig 2. Similar averages centered on randomly chosen positions in SPIRE images do not show this deficit.

3. THEORETICAL GROUNDS

Gravitational lensing conserves surface brightness and therefore does not alter the mean intensity of the extragalactic background light at any wavelength. However, this statement applies only when all sources are kept in calculating the intensity profile and when averaged over many directions through the cluster – for some configurations of the background sky unusually bright images can be found. The measurement reported here involves
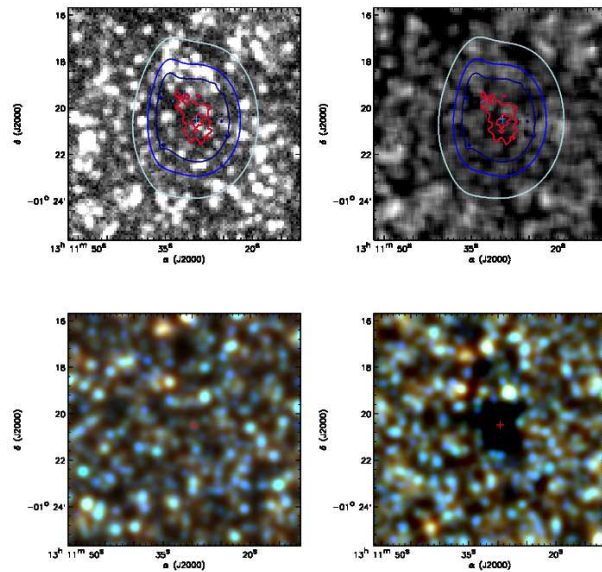
Figure 1. Lensed and field images of the CIB from SPIRE. The upper left-hand panel shows the $250\,\mu$m Abell 1689 image, and the upper right-hand panel shows the same image after detected sources have been subtracted. Because the detection threshold is equal to the confusion limit and the noise is not uniform over the image, at the high contrast level of the right hand image $\sim 1\sigma_{\rm conf}$ noise fluctuations are visible towards the edges of the map. The colored contours show the iso-magnification levels from the gravitational lensing model for a source at $z = 1.5$ with $\mu < 0$ enclosed by the central red contours and $\mu = \{3, 2, 1.5\}$ in lightening shades of blue. The lower two panels show SPIRE 3-band false color simulations of the CIB to $S \lesssim 100$ nJy, not including noise. The lower left-hand panel is a image of the CIB without lensing, while the right-hand panel shows the same background that has been propagated through a lens model for Abell 1689; no emission from the cluster or SZ effect is included.

the removal of bright detected sources, which leads to a situation where lensing shows a profile that does not conserve intensity. This does not imply that the total number of photons and therefore intensity is not conserved, as discussed in Refregier & Loeb (1997), since detected sources are removed.

When viewed through a lensing cluster imposing a magnification μ on background sources, a background source with flux density S is magnified such that the observed flux density is $S' = \mu S$. The resulting increase in the flux density is accompanied by a corresponding decrease in the projected surface density of galaxies; the observed number density of sources through the lens is modified to be $N' = N/\mu$. The overall effect of this is to modulate existing fluctuations in the background source field. Using the parametrization that the intrinsic number count of the faint background sources scales as $dN/dS \propto S^{-\Gamma}$, the differential number counts lensed through the cluster become $dN'/dS' \propto \mu^{\Gamma-2}S^{-\Gamma}$. The differential counts imaged through the cluster are either decreased or increased depending on whether the intrinsic counts have a slope Γ smaller than or greater than 2. If sources are not removed from the image, the total CIB surface brightness is conserved Refregier & Loeb (1997).

The observations reported here do not constrain the exact number counts of sources or the difference of the counts of sources through and away from the cluster. One reason for this is that the observations are sampled
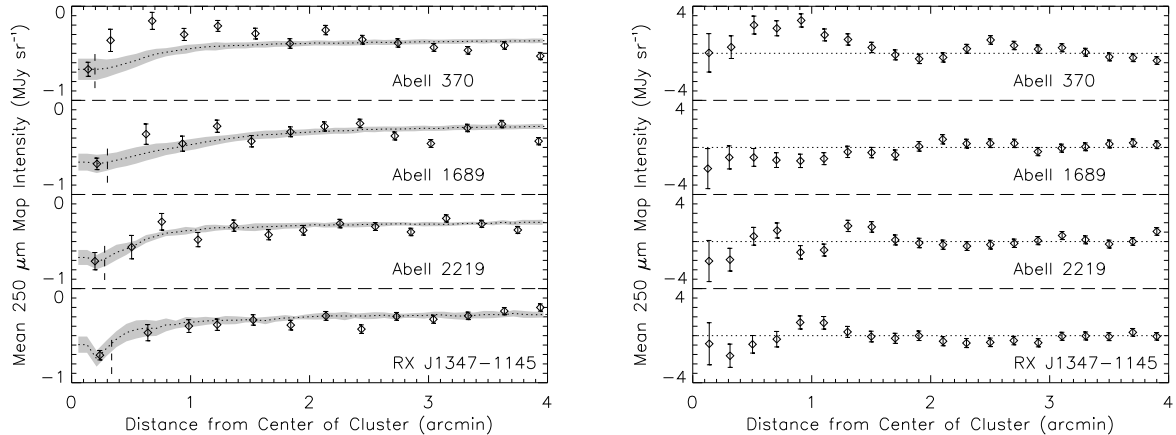
Figure 2. Intensity profiles towards four clusters, illustrating gravitational lensing of the CIB. The left hand plots show the mean flux density in $0.25'$-wide annular bins for each cluster after all detected sources have been removed. The central data point is constructed from all map pixels within the effective radius characteristic of the clusters' critical lines (marked by the vertical dashed lines). At larger radii, the data points represent uncertainty-weighted averages starting at the characteristic critical line radius. The mean level of each simulated map is constructed to be zero before source subtraction and is reduced by $\sim 0.3\,\mathrm{MJy\,sr^{-1}}$ after a large fraction of the CIB has been detected as sources and removed; the offset varies between targets depending on how many sources are removed. The uncertainties on the data points are photometric accuracy of the measurements rather than the precision with which the mean should differ from the model. Dotted lines and grey contours show the mean and standard deviation of our sky model, calculated from simulations of the interaction of the CIB and each lensing cluster, passed though our data analysis pipeline. The right hand plots show the annular averages of the raw cluster images with no source extraction, which highlight the structure of the surface brightness which is subtracted by removing detected sources.

by the limited angular resolution of the SPIRE instrument, which results in a blending of the faintest sources. The effects of limited-resolution observations of the intensity profile of background sources through the cluster are described in Blain (1997) and Blain (2002). High resolution observations with ALMA will allow one to more precisely measure the difference in the counts away from and through the cluster.

4. NUMERICAL SIMULATION

We can use detailed lensing models of these well-studied clusters and models of the source counts and redshift distributions of the sources which comprise the CIB to generate numerical simulations of the observed sky brightness, and explore how the amplitude of an observed deficit depends on source model parameters. To simulate the sub-mm background, we use the model described in Béthermin et al. (2011), which is tuned to match a variety of observed number counts dN/dS and is forced to integrate to the total intensity of the CIB (Lagache et al. 2000). The model associates both a spectral shape and redshift to each source, down to $z = 0$. These simulations do not include coherent clustering of the galaxies which comprise the sub-mm background, which is a small effect on the scales of interest here ($\theta < 3$ arcminutes; Viero et al. 2012). Poisson noise is modeled by the simulation, and naturally accounts for the cosmic variance one would expect in the real sky. The simulated images have area 0.25 deg^2 and contain $\sim 5 \times 10^4$ sources to source fluxes $S_{\mathrm{min}} = 50\,\mathrm{nJy}$. In the parametrization $dN/dS \propto S^{-\Gamma}$, the faint end number counts of this model have $\Gamma \sim 1.5$, so they integrate to a finite value of the CIB.

These simulated backgrounds are then lensed using LENSTOOL models (Kneib et al. 1996; Jullo et al. 2007; Jullo & Kneib 2009), which are built using optical measurements of strong lensing in the cluster fields, modeling all of the known high-magnification images mea-

sured for each cluster. The LENSTOOL models replicate all of the phenomenology arising from the complex dark-matter potentials of each cluster, including multiple images, giant arcs, and so on. Gravitational lensing is achromatic, so the same lens model applies at all wavelengths. Sources with $z < z_c$ are included in the simulated sky map, but are not lensed; all the sources with $z > z_c$ are lensed from redshift planes discretized into $\delta z = 0.1$ steps. An example of one such simulation is shown in the bottom panels of Fig. 1. Excluding other sources of emission, the central surface brightness deficit is evident in the modeled image in all three SPIRE bands.

These simulations show that three factors contribute to the effect reported here: (1) the sizes and typical lensing amplification factors of clusters; (2) the number densities and redshifts of the sources responsible for the CIB; and (3) the sensitivity and beam size of SPIRE. These combine so that when we examine the lensed cores of SPIRE images of cluster fields and remove all reasonably significant sources, we are left with deficits in the surface brightness of the sky in small regions near the cluster center.

In order to compare the data to the simulations, we use the same procedure discussed above on simulations of the cluster targets. In these simulations, instrumental noise with the same amplitude as measured in the data is inserted into the simulated, lensed cluster images, and these images are propagated through an identical detection/subtraction procedure as the real data, resulting in the grey bands in Fig. 2 which represent the mean and standard deviation of the model results drawn from 100 realizations of the background sky that capture the variance of the lensing deficit due to different background configurations and reflect the range of possible deficit shapes and amplitudes arising from our ignorance of the exact configuration of the background sources which give rise to the deficit.

A potential concern is whether simulating sources to $S \sim 50 \, \mathrm{nJy}$ is sufficient for the modeling result to converge. To check this, we have performed simulations where sources are not included below $S_{\min}$. By $S_{\min} = 10 \, \mu\mathrm{Jy}$ the map is densely populated and the effect has converged, and including fainter sources does not have an appreciable effect on the amplitude of the deficit. This is because sources below $10 \, \mu\mathrm{Jy}$ are rarely boosted above the 1σ detection threshold and so do not reate a net deficit after source removal.

To investigate the dependence of the deficit on the background number counts, we perform simulations drawn from the measured counts presented in Glenn et al. (2010) similar to the calculations in Ford et al. (2012). The slope of the faint end for $0.1 < S < 2 \, \mathrm{mJy}$ are varied in the range $1.0 \leq \Gamma \leq 3.0$, bracketing the nominal value of $\Gamma = 1.65$ which accounts for the full FIRAS background (Fixsen et al. 1998; Lagache et al. 2000). As can be seen in Fig. 3, for shallow slopes, the surface density of sources is small enough to produce zero flux in the center of clusters. For steeper slopes, the probability that a source falls behind the center of the cluster image is no longer small and the surface brightness increases. Existing constraints on the brightness of the CIB at $250 \, \mu\mathrm{m}$ exclude $\Gamma > 2.3$ at 2σ in this range (Fixsen et al. 1998).
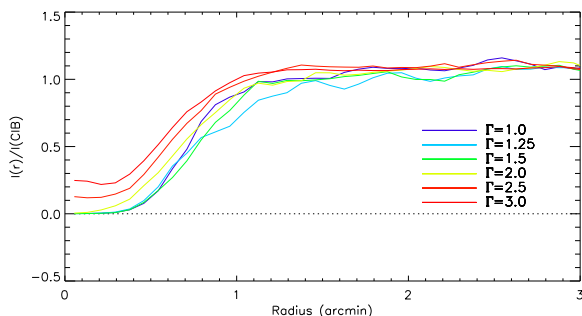
Figure 3. Effect of the slope of the faint end source counts Γ on the lensing deficit. The surface brightness of the sky is averaged into annular bins centered on the cluster and expressed as a ratio of the brightness at radius r to the overall sky surface brightness. For slopes similar to that inferred from other measurements ($\Gamma \approx 1.5$), the center of our modeled clusters has an expectation value of zero; as the slope is increased, the probability of a source falling into the caustic region is increased until the deficit begins to be filled in.

5. MEASUREMENT OF THE CIB AT 250 MICRONS

According to our simulations using the Béthermin et al. (2011) model, statistically the central region of these clusters' images have zero surface brightness from lensed sources. At $250 \, \mu\mathrm{m}$, emission from sources within the central arcminute of clusters tends to be faint. Therefore a situation arises where the cluster itself is invisible, the probability of a foreground source coinciding with the cluster center is small, and the background is lensed by the cluster, so that no sources of emission exist in the center of the cluster. If this region has zero surface brightness, as this model suggests, we can use it to tie the image to an absolute zero point.

Of course, if the above assumption is incorrect, any sources of emission local to the cluster center – for example, from the BCG or the SZ effect – will bias the mea-

surement to lower inferred surface brightness. Though only a $< 0.1\%$ fractional contamination in the $250 \, \mu\mathrm{m}$ SPIRE band, the SZ effect is significant at longer sub-mm wavelengths (Zemcov et al. 2007; Zemcov et al. 2010) so we defer reporting the CIB inferred from the two longer wavelength SPIRE bands to future work where we model the intra-cluster medium (ICM) in each cluster. Sub-mm emission associated with the central region of target clusters is known (Rawle et al. 2012); for example, in the HerMES sample (but excluded from this work) Abell 1835 and Abell 2390 are both known to host Brightest Cluster Galaxies (BCGs) with sub-mm fluxes of many mJy. Because of this potential bias, the lensing deficit produces a lower limit to the CIB. To check for contamination from galaxies within the critical region, we use *Spitzer*-MIPS $24 \, \mu\mathrm{m}$ data. No BCGs are obvious in the SPIRE images of the four clusters, but we can use the $24 \, \mu\mathrm{m} - 250 \, \mu\mathrm{m}$ BCG flux density ratio measured by Rawle et al. (2012) to estimate an additional one-sided, positive-going uncertainty to the central zero point in each image. This corresponds to a 1σ value of $0.4 \, \mathrm{mJy}$ per beam at the position of the BCG. We do not detect other $24 \, \mu\mathrm{m}$ sources associated with the cluster in the central deficit region. Diffuse dust emission associated with the ICM has never been detected, but from predictions we expect this kind of emission to be at least an order of magnitude smaller than the surface brightness of the lensing deficit at $250 \, \mu\mathrm{m}$ (Popescu et al. 2000).

To determine the absolute intensity of the CIB, the average of each map in its central region is used to generate a zero point for the image. The mean brightness of the resulting image, excluding the central region, is then computed. To estimate the uncertainty associated with each measurement, we compute the quadrature sum of the statistical uncertainty of the maps as traced by the standard deviation of the pixels in the central region (Stat. $\delta I_{250 \, \mu\mathrm{m}}$), the one-sided uncertainty from the BCG emission (BCG $\delta I_{250 \, \mu\mathrm{m}}$), the uncertainty from the simulations associated with the configuration of the background source (Model $\delta I_{250 \, \mu\mathrm{m}}$), and the 5 % absolute calibration uncertainty of SPIRE (Abs. Cal. $\delta I_{250 \, \mu\mathrm{m}}$). We estimate the Eddington bias associated with the effect of subtracting sources from the maps before computing the mean of the central region by comparing simulations including and excluding simulated noise, resulting in an estimate of $\delta I < 0.03 \, \mathrm{MJy} \, \mathrm{sr}^{-1}$ for the Eddington bias on the sample. Table 1 lists the areas of negative magnification in each target, the inferred CIB brightness for each of the four cluster fields that pass all of the selection cuts, and the uncertainty budget associated with these measurements. The statistical-uncertainty weighted mean of this value, $0.69^{+0.12}_{-0.07} \, \mathrm{MJy} \, \mathrm{sr}^{-1}$, is the inferred brightness of the CIB at $250 \, \mu\mathrm{m}$ from the lensing deficit method. This value is consistent with the FIRAS values determined by Puget et al. (1996), Fixsen et al. (1998), and Lagache et al. (2000) in the same band within 1σ.

6. DISCUSSION

We have detected an interesting new phenomenon which is due to the properties of the sub-mm background and gravitational lensing in massive clusters. This deficit in the measured surface brightness constrains the smallest allowable surface brightness of the CIB and so is another way to limit its absolute brightness, adding to a

Table 1
Lensing deficit CIB limits & error budget.

Cluster	$\sum \Omega$ (Ω_s)	CIB $I_{250\,\mu m}$ (MJy sr^{-1})	Stat. $\delta I_{250\,\mu m}$ (MJy sr^{-1})	Model $\delta I_{250\,\mu m}$ (MJy sr^{-1})	BCG $\delta I_{250\,\mu m}$ (MJy sr^{-1})	Abs. Cal. $\delta I_{250\,\mu m}$ (MJy sr^{-1})	Total $\delta I_{250\,\mu m}$ (MJy sr^{-1})
Abell 370	3.0	0.67	±0.08	±0.11	+0.05	±0.03	−0.14, +0.15
Abell 1689	7.5	0.68	±0.06	±0.09	+0.05	±0.03	−0.11, +0.12
Abell 2219	3.3	0.71	±0.09	±0.08	+0.05	±0.04	−0.13, +0.14
RX J 1347−1145	11.3	0.71	±0.05	±0.09	+0.05	±0.04	−0.11, +0.12
Total	25.1	0.69	±0.03	±0.05	+0.09	±0.04	−0.07, +0.12

list which includes $P(D)$ analyses, stacking, and source counting, in addition to direct photometric measurement. Furthermore, in principle the presence of this deficit places interesting constraints on the faint end of the number counts, although larger samples and comprehensive modeling are required to convert measurements to source count constraints.

Because gravitational lensing is achromatic, this effect occurs in all of the SPIRE bands. Other instruments working at sub-mm and mm wavelengths like ACT/SPT and CCAT should also be able to measure this deficit effect, assuming that the background in question is sufficiently far behind the lensing cluster, and that the instrumentation is sensitive to sources at levels similar to SPIRE's with enough angular resolution to resolve the central region of clusters. In addition, this effect produces a complicated, spatially structured CIB surface brightness distribution which is a potential foreground for high resolution SZ effect measurements at longer wavelengths.

REFERENCES

Béthermin, M., Dole, H., Lagache, G., Le Borgne, D., & Penin, A. 2011, A&A, 529, A4
Blain, A. W. 1997, MNRAS, 290, 553
—. 2002, MNRAS, 330, 219
Etherington, I. M. H. 1933, Philosophical Magazine, 15, 761
Fixsen, D. J., Dwek, E., Mather, J. C., Bennett, C. L., & Shafer, R. A. 1998, ApJ, 508, 123
Ford, J., et al. 2012, ApJ, 754, 143
Glenn, J., et al. 2010, MNRAS, 409, 109
Griffin, M. J., et al. 2010, A&A, 518, L3
HerMES Collaboration et al. 2012, ArXiv e-prints
Jullo, E., & Kneib, J.-P. 2009, MNRAS, 395, 1319
Jullo, E., Kneib, J.-P., Limousin, M., Elíasdóttir, Á., Marshall, P. J., & Verdugo, T. 2007, New Journal of Physics, 9, 447
Kneib, J.-P., Ellis, R. S., Smail, I., Couch, W. J., & Sharples, R. M. 1996, ApJ, 471, 643
Lagache, G., Haffner, L. M., Reynolds, R. J., & Tufte, S. L. 2000, A&A, 354, 247
Levenson, L., et al. 2010, MNRAS, 409, 83
Nguyen, H. T., et al. 2010, A&A, 518, L5
Oliver, S. J., et al. 2010, A&A, 518, L21
Ott, S., et al. 2006, in Astronomical Society of the Pacific Conference Series, Vol. 351, Astronomical Data Analysis Software and Systems XV, ed. C. Gabriel, C. Arviset, D. Ponz, & S. Enrique, 516
Pilbratt, G. L., et al. 2010, A&A, 518, L1
Popescu, C. C., Tuffs, R. J., Fischera, J., & Völk, H. 2000, A&A, 354, 480
Puget, J.-L., Abergel, A., Bernard, J.-P., Boulanger, F., Burton, W. B., Desert, F.-X., & Hartmann, D. 1996, A&A, 308, L5
Rawle, T. D., et al. 2012, ApJ, 747, 29
Refregier, A., & Loeb, A. 1997, ApJ, 478, 476
Schneider, P., Ehlers, J., & Falco, E. E. 1992, Gravitational Lenses
Smith, A. J., et al. 2012, MNRAS, 419, 377
Turner, E. L. 1980, ApJ, 242, L135
Viero, M. P., et al. 2012, ArXiv e-prints
Zemcov, M., Borys, C., Halpern, M., Mauskopf, P., & Scott, D. 2007, MNRAS, 376, 1073
Zemcov, M., et al. 2010, A&A, 518, L16+
Zitrin, A., Broadhurst, T., Rephaeli, Y., & Sadeh, S. 2009, ApJ, 707, L102